

Crystal structure of human mitochondrial NAD(P)⁺-dependent malic enzyme: a new class of oxidative decarboxylases

Yingwu Xu¹, Girija Bhargava¹, Hao Wu², Gerhard Loeber³ and Liang Tong^{1*}

Background: Malic enzymes catalyze the oxidative decarboxylation of malate to pyruvate and CO₂ with the concomitant reduction of NAD(P)⁺ to NAD(P)H. They are widely distributed in nature and have important biological functions. Human mitochondrial NAD(P)⁺-dependent malic enzyme (mNAD-ME) may have a crucial role in the metabolism of glutamine for energy production in rapidly dividing cells and tumors. Moreover, this isoform is unique among malic enzymes in that it is a cooperative enzyme, and its activity is controlled allosterically.

Results: The crystal structure of human mNAD-ME has been determined at 2.5 Å resolution by the selenomethionyl multiwavelength anomalous diffraction method and refined to 2.1 Å resolution. The structure of the monomer can be divided into four domains; the active site of the enzyme is located in a deep cleft at the interface between three of the domains. Three acidic residues (Glu255, Asp256 and Asp279) were identified as ligands for the divalent cation that is required for catalysis by malic enzymes.

Conclusions: The structure reveals that malic enzymes belong to a new class of oxidative decarboxylases. The tetramer of the enzyme appears to be a dimer of dimers. The active site of each monomer is located far from the tetramer interface. The structure also shows the binding of a second NAD⁺ molecule in a pocket 35 Å away from the active site. The natural ligand for this second binding site may be ATP, an allosteric inhibitor of the enzyme.

Introduction

Malic enzyme (ME; EC 1.1.1.40) catalyzes the oxidative decarboxylation of L-malate to pyruvate with the concomitant reduction of the cofactor NAD⁺ or NADP⁺ [1–5]. In addition to NAD(P)⁺, the enzyme also requires divalent cations (Mg²⁺ or Mn²⁺) as cofactors.



MEs can be divided into three groups on the basis of their requirement for the dinucleotide cofactor: NAD⁺- or NADP⁺-dependent enzymes that can only use NAD⁺ or NADP⁺ as the cofactor, respectively, and NAD(P)⁺-dependent ‘dual-specificity’ enzymes that can use both NAD⁺ and NADP⁺ as cofactor.

ME activity was first isolated from pigeon liver [6]. Since then, MEs have been found in most living organisms, including bacteria, yeast, fungi, plants, humans and other animals. The cDNA sequences of more than 40 different MEs have been determined. In mammals, three isoforms of ME have been identified [7]: cytosolic NADP⁺-dependent ME (cNADP-ME), mitochondrial NADP⁺-dependent ME (mNADP-ME), and mitochondrial NAD(P)⁺-dependent ME (mNAD-ME). mNAD-ME can use both NAD⁺ and

Addresses: ¹Department of Biological Sciences, Columbia University, New York, NY 10027, USA, ²Department of Biochemistry, The Weill Medical College of Cornell University, New York, NY 10021, USA and ³Boehringer Ingelheim Austria R&D, Dr Boehringer-Gasse 5-11, A-1121 Vienna, Austria.

*Corresponding author.
E-mail: tong@como.bio.columbia.edu

Keywords: allosteric interactions, cofactor specificity, glutamine metabolism, protein folds

Received: 11 March 1999
Revisions requested: 7 April 1999
Revisions received: 14 April 1999
Accepted: 15 April 1999

Published: 2 July 1999

Structure August 1999, 7:877–889
<http://biomednet.com/elecref/0969212600700877>

© Elsevier Science Ltd ISSN 0969-2126

NADP⁺ as the cofactor (dual-specificity), but prefers NAD⁺ under physiological conditions.

As suggested by their wide distributions in nature, MEs have important biological functions. The biochemical reaction catalyzed by ME produces pyruvate, CO₂ and NAD(P)H, and different biological processes can be supported by these products. For example, because of the CO₂ production, ME has a crucial role in the photosynthetic reactions in tropical C4 plants [8]. Studies of this ME may also help delineate the evolutionary process for the photosynthetic pathway in C4 plants [9,10]. In fungi and other organisms, an ME, via the NADPH product, is believed to have lipogenic functions [11]. Similarly, the cNADP-ME isoform in mammals is involved in the generation of NADPH and the biosynthesis of fatty acids and steroids in liver and adipose tissues [8]. cNADP-ME is under dietary control and can be induced by a carbohydrate-rich diet or thyroid hormones. A thyroid response element is present in the promoter region of the cNADP-ME gene [12]. cNADP-ME may also have a role in microsomal drug detoxification [13].

In comparison, the mNAD-ME isoform, via the NADH and pyruvate products, is believed to have an important role in energy production in rapidly proliferating tissues

(e.g. spleen, thymus, mucosal cells of small intestine), and particularly in tumors [3,14]. mNAD-ME may be crucial for the metabolism of glutamine, which is the most abundant single amino acid in plasma, tissues and cell culture media [15]. Glutamine is the major energy source of many tumor cells [13,14], many of which do not have a strict requirement for glucose for energy production [16]. A possible pathway for the metabolism of glutamine to pyruvate has been proposed [15] (GL, unpublished results).

Glutamine \rightarrow glutamate \rightarrow α -ketoglutarate \rightarrow succinate \rightarrow fumarate \rightarrow malate \rightarrow pyruvate

This pathway has been termed 'glutaminolysis' [15], in analogy to the glycolysis pathway that converts glucose to pyruvate. The part of the pathway that converts α -ketoglutarate to malate is actually in the citric acid cycle (Krebs cycle) [8]. The next reaction in the citric acid cycle is the oxidation of malate to produce oxaloacetate, catalyzed by malate dehydrogenase (MDH). In the glutaminolysis pathway, however, malate is converted to pyruvate by oxidative decarboxylation, which is catalyzed by ME.

MEs are generally homotetramers, with monomers containing ~550 amino acid residues and having molecular weights of ~60 kDa. These enzymes are therefore much larger than the dehydrogenases (including MDH). Heterodimeric MEs have been identified from some plants [17] and the thermophilic bacterium *Bacillus stearothermophilus* [18]. As expected from their important biological functions, the amino acid sequences of MEs from various organisms show significant conservation. For example, human, rat and mouse cNADP-ME share 90% sequence identity [7]. Human mNAD-ME shares 55% sequence identity with human mNADP-ME or cNADP-ME. Another remarkable example of the high degree of conservation is that the human mNADP-ME and the maize chloroplast NADP-ME share 47% amino acid sequence identity [7].

The amino acid sequences of ME contain two copies of the dinucleotide-binding signature motif GXGXXG/A (single-letter amino acid code) [19], corresponding to 168-GLGDLG-173 and 311-GAGEAA-316 in mNAD-ME. Apart from these two motifs, ME does not show recognizable sequence homology to other proteins, for example the dehydrogenases (including MDH) and the decarboxylases. The crystal structures of three oxidative decarboxylases are known: 6-phosphogluconate dehydrogenase (6PGDH) [20], isocitrate dehydrogenase (ICDH) [21] and isopropylmalate dehydrogenase (IpMDH) [22]. ICDH and IpMDH have detectable amino acid sequence homology (25% identity) and have similar backbone folds. The sequence and structure of 6PGDH share no homology with those of ICDH or IpMDH. The amino acid sequences of ME do not show any homology to these three proteins or any other oxidative decarboxylases.

Therefore, MEs may have a distinct backbone structure and form a new class of oxidative decarboxylases.

We have chosen to study human mNAD-ME as a model system to obtain greater understanding of the biochemistry and biology of this important class of enzymes. In addition, the dual-specificity of mNAD-ME offers the unique opportunity of studying the same enzyme bound to NAD⁺ and NADP⁺. Such studies should increase our understanding of the structural basis for cofactor selectivity [19,23–25]. Furthermore, mNAD-ME is distinct from the other two mammalian ME isoforms in that it is a cooperative enzyme with respect to the substrate malate, and because its catalytic activity is allosterically controlled by fumarate (and to a lesser extent succinate) as an activator and by ATP as an inhibitor [26]. Fumarate and ATP have no effects on the catalytic activity of cNADP-ME and mNADP-ME. As a first step in these studies, we report here the crystal structure of human mNAD-ME in complex with NAD⁺ at 2.1 Å resolution. The crystallization of ME from rat liver [27] and the nematode *Ascaris suum* [28] have been published, however, no structural information has so far been reported on any ME.

Results

The structure of the monomer

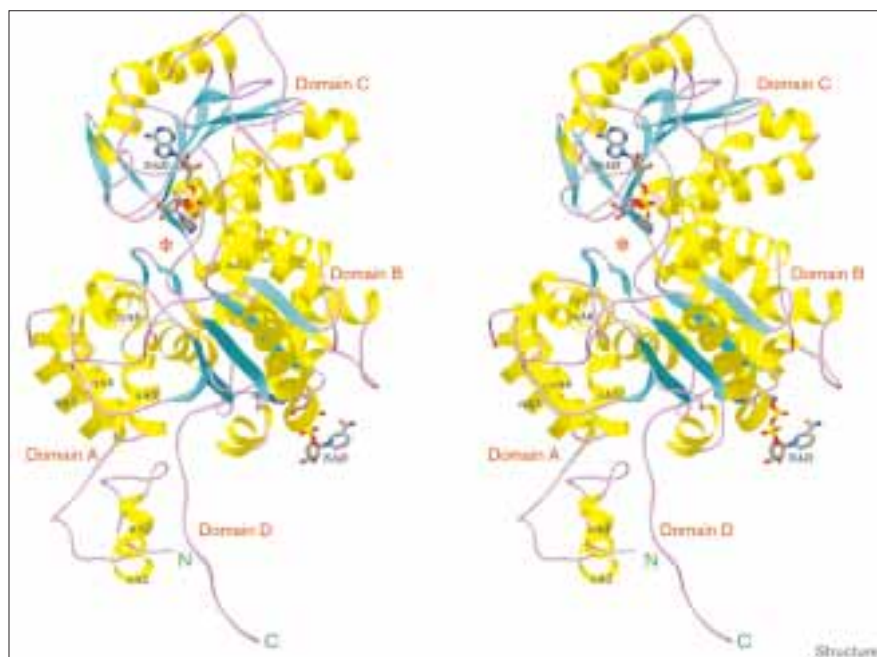
The structure of human mNAD-ME was determined at 2.5 Å resolution by the selenomethionyl multiwavelength anomalous diffraction (MAD) method [29] and subsequently refined to 2.1 Å resolution. The positions of 28 selenium sites were successfully located based on the MAD analysis, which represents one of the largest number of sites that have been solved with the F_A approach as implemented in the MADSYS program [29]. The current atomic model contains residues 23–573 for each of the two monomers in the asymmetric unit. Four residues at the N terminus together with 11 at the C terminus of the protein are disordered. Two NAD⁺ molecules are associated with each monomer of mNAD-ME. The crystallization solution also contained Mg²⁺ and tartronate, a substrate analog inhibitor; however, it appears that they are not bound to the enzyme in the crystal.

The two monomers of mNAD-ME in the asymmetric unit have very similar conformations: the root mean square (rms) distance between the 551 equivalent C α positions is 0.34 Å. Three regions show distances of ~1 Å (residues 298–304, 505–509 and 568–573); the latter region comprises residues at the tetramer interface. The two monomers are related by a twofold rotation (179.4°) along a direction perpendicular (90.6°) to the crystal twofold (c) axis. A tetramer of the enzyme is generated by this crystallographic twofold axis.

The structure of the mNAD-ME monomer can be divided roughly into four domains (A, B, C and D) (Figure 1).

Figure 1

Stereoview schematic drawing of the mNAD-ME monomer [63]. The β strands are shown in cyan, α helices in yellow, and the connecting loops are in purple. The four domains of the structure are labeled. The two NAD⁺ molecules bound to the enzyme are shown as stick models colored according to atom type: carbon gray, oxygen red, nitrogen blue, and phosphorus yellow. The helices in domain A are labeled. The putative active site of the monomer is indicated by the red star.



Domain A consists of residues 23–130 and is mostly helical (α A1– α A6). Helix α A6 has a bulge in the middle, resulting in a sharp turn in the direction of the helix. This might be due to the presence of the strictly conserved Pro109 and Pro114 residues. Domain B comprises two segments of the polypeptide chain, residues 131–277 and 467–538 (Figure 2a). The distance between the C α atoms of residues 278 and 467 is 7.6 Å, suggesting that residues 278–466 (domain C) can be considered as an inserted cassette for the second domain. Domain C (residues 278–466) comprises a parallel β sheet (β C1– β C7) surrounded by helices on both sides (α C0– α C5). The topology of this domain is similar to the canonical Rossmann fold [30], although there are also significant variations (Figure 2b). The last domain (residues 539–573), contains one helix followed by a long extended structure that protrudes away from the monomer. The structure of 6PGDH also contains a Rossmann fold domain, although it is located at the N terminus [20]. Overall, the backbone fold of mNAD-ME shows no similarity to that of ICDH, IpMDH or 6PGDH. MEs therefore represent a new class of oxidative decarboxylases.

A new fold in domain B

Domain B contains a parallel five-stranded β sheet (β B1– β B5) surrounded by helices on both sides (α B1 through α B8; Figure 2a). The parallel β sheet has the connectivity 1,3,2,4,5 (Figure 2a). Searches for structural homologs, with the program DALI [31] and the SCOP data base [32], have so far failed to reveal another protein structure with a similar β sheet. Therefore, this domain of ME may represent a new polypeptide backbone fold for a

five-stranded parallel β sheet. Without the first strand, the remaining four-stranded parallel β sheet, with the connectivity 2,1,3,4, has been found in many protein structures.

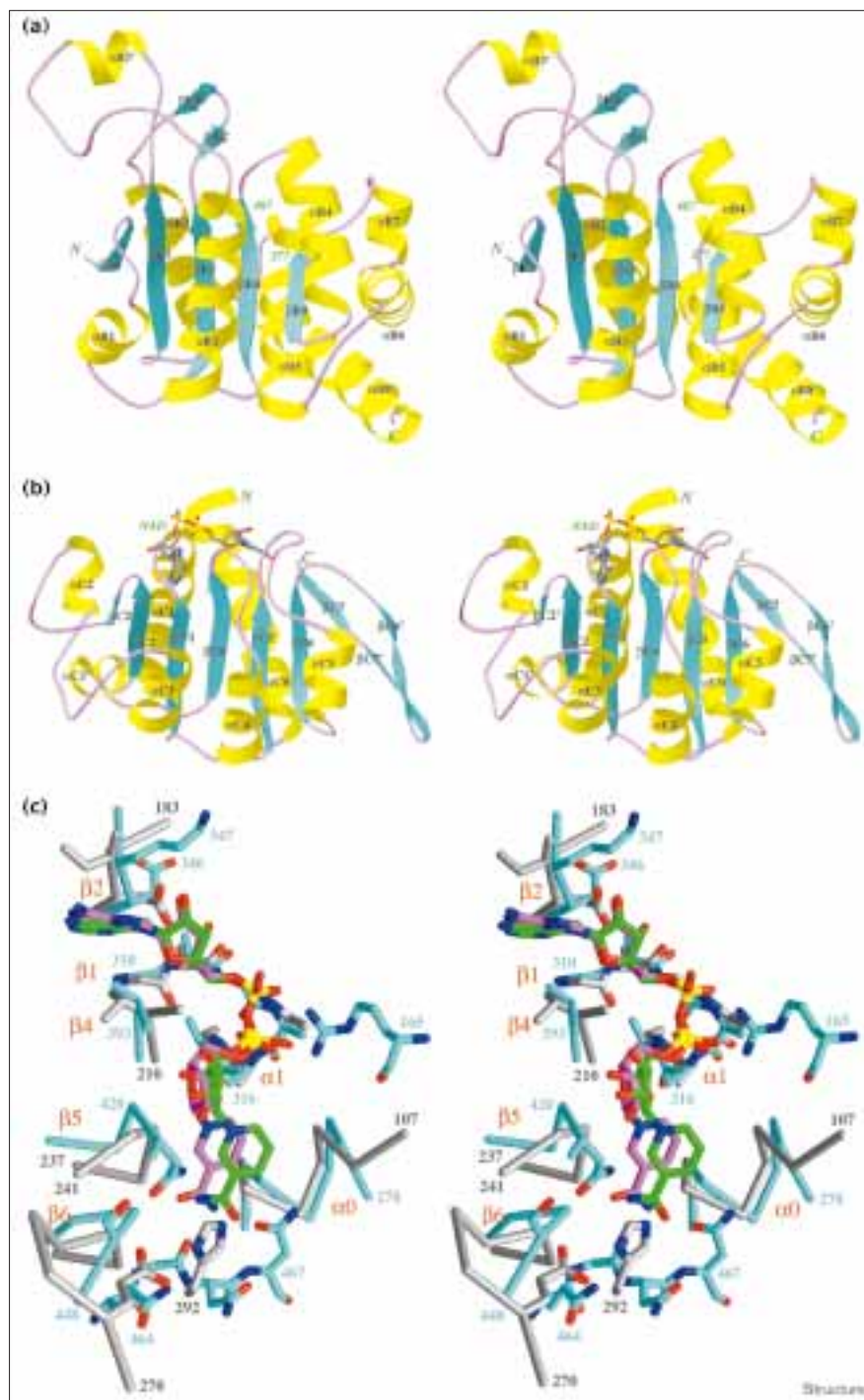
This domain is made up of two segments of the polypeptide chain. The entire parallel β -sheet structure, together with five helices, is enclosed in the first segment. The second segment contains one helix, α B5, that packs against one face of the β sheet and shields it from the solvent. Helices α B5, α B6 and α B8 form an antiparallel bundle, with a hydrophobic core (Figure 2a).

There is a short β -hairpin structure (β B2'– β B3') between strand β B2 and helix α B2. The residues in this region, 160-TDGERILGLGDLG-173, correspond to one of the highly conserved sequence motifs in MEs (Figure 3). This region also contains the first GXGXXG motif in MEs, 168-GLGDLG-173, with the first glycine (Gly168) at the tip of the β hairpin. Contrary to expectations from the sequence analysis, the residues in this motif are not involved in NAD⁺ binding. This β -hairpin structure is near the nicotinamide ring of the NAD⁺ molecule associated with domain C, however, and may therefore be involved in substrate binding by the enzyme.

A Rossmann fold in domain C

The second dinucleotide-binding signature motif, 311-GAGEAA-316, is located between β C1 and α C1 in domain C (Figure 2b), similar to the location of this motif in other Rossmann fold structures [19,30]. Strongest similarity was found between the structure of this domain and

Figure 2



Domains of the mNAD-ME structure.

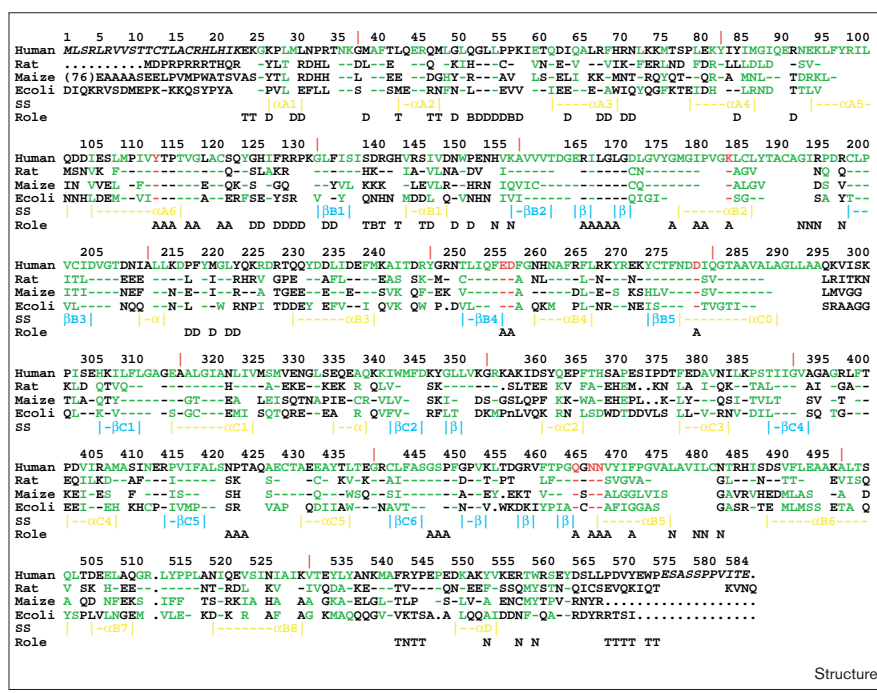
(a) Stereoview schematic drawing of the structure of domain B of human mNAD-ME. The β strands and α helices are labeled; the color-code is the same as in Figure 1. Residues at the end of the first polypeptide segment and the beginning of the second segment are labeled in green. **(b)** Stereoview schematic drawing of the structure of domain C of human mNAD-ME. The β strands are numbered according to the consensus with other Rossmann fold structures. Strand β 3 is absent in the structure of mNAD-ME. The bound NAD⁺ molecule is shown as a stick model and labeled. **(c)** Stereoview comparison of the structures of mNAD-ME and D-3-phosphoglycerate dehydrogenase (PDB accession code 1PSD) [33] near the NAD⁺ molecule. The C α traces, together with some sidechains involved in NAD⁺ binding, are shown for mNAD-ME (carbon atoms in cyan) and 1PSD (in gray). The NAD⁺ molecule in the mNAD-ME structure is shown with carbon atoms in purple and the NAD⁺ molecule in 1PSD is in green. The locations of some of the secondary structure elements of the Rossmann fold are labeled in red. The Glu269–His292 pair of residues is conserved in many dehydrogenases and is involved in catalysis [64].

the Rossmann fold domain of D-3-phosphoglycerate dehydrogenase (Protein Data Bank [PDB] entry code 1PSD) [33], and the related NAD-dependent formate dehydrogenase (2NAD) [34], D-glycerate dehydrogenase (1GDH) [35] and D-2-hydroxyisocaproate dehydrogenase (1DXY) [36]. For example, a structural alignment between domain C of mNAD-ME and 1PSD brought 119 C α atoms into

equivalent positions (within a distance of 3.5 Å), and the rms deviation between these C α positions was 1.9 Å. The maximum amino acid sequence identity between mNAD-ME and other Rossmann fold domains based on the structural alignment was 15%, indicating a high degree of structural conservation in the absence of sequence conservation for the Rossmann fold.

Figure 3

Sequence alignments of human mNAD-ME, rat cNADP-ME, maize ME and the putative ME of *E. coli*. The red vertical bars represent the locations of introns in the genomic sequence of rat ME [65]. A dot represents a deletion, and a dash represents an identity to the sequence of human mNAD-ME. The secondary structure elements in mNAD-ME are indicated (SS). Residues colored in green are those that are buried (with less than 25% accessible surface area) in the monomer. Residues having special functional roles are indicated: D or T, a residue at the dimer or tetramer interface; B, a residue at both dimer and tetramer interfaces; A, a residue at the active site; N, a residue at the second NAD⁺-binding site. Residues colored in red may be important for catalysis. Residues shown in italics are not observed in the current structure; of these, residues 2–19 (containing the mitochondrial targeting sequence) are not included in the expression construct [3,41].



Domain C of mNAD-ME starts with a long helix (α C0; residues 278–298) that packs against the β sheet (Figure 2b); residue Asp279 near the N terminus of this helix is involved in binding the divalent cation (see below). This helix is observed in most other Rossmann fold structures and should be considered as an integral component of the Rossmann fold, as it shields part of the central β sheet from solvent. The residues that form this helix have, however, been found in different regions of primary sequence of the various proteins — both N- and C-terminal to the central β sheet of the Rossmann fold. In 1PSD (and related enzymes 2NAD, 1GDH, 1DXY), glutamate dehydrogenase (1K89) [37] and leucine dehydrogenase (1LEH) [38], residues in this helix are located N-terminal to the β sheet, as also seen here with mNAD-ME. In other Rossmann fold structures, for example lactate dehydrogenase (1LDM) [39], this helix is formed by residues C-terminal to the β sheet, although the position and the orientation of the helix is conserved.

There are recognizable differences between the backbone fold of domain C of mNAD-ME and the canonical Rossmann fold. The strand order for the six-stranded parallel β sheet in a Rossmann fold is normally 3,2,1,4,5,6. In the structure of mNAD-ME, strand β C3 is absent, however (Figure 2b). This absence is possibly due to the insertion of an additional helix between strands β C1 and β C2, residues 334–339 (α C1'), that takes up part of the position of β C3. Residues 348–350 after strand β C2 form a short β -hairpin segment (β C2') that makes three hydrogen bonds with

residues in strand β C2 (Figure 2b). An antiparallel strand at the β 3 position was observed in the structure of glutamate dehydrogenase [37]. An additional strand (β C7) is hydrogen bonded to β C6 in a parallel fashion in the structure of mNAD-ME, as seen in many other structures. In the current structure, there is a β hairpin between strands β C6 and β C7. However, many of the residues in this β hairpin have rather weak electron density (especially residues 454–458), and this region corresponds to deletions in the amino acid sequences of many other MEs (Figure 3).

An NAD⁺ molecule is associated with domain C, at a position similar to that of NAD⁺ in other Rossmann fold domains. The ADP portion of the cofactor in the current structure is in excellent agreement with that in 1PSD, although the planes of the two nicotinamide rings are separated by ~ 2.6 Å (Figure 2c). The hydroxyl groups on the adenine ribose are recognized by an aspartate residue in 1PSD and many other Rossmann fold structures. The presence of an acidic residue at this position (at the end of strand β 2) is believed to confer NAD⁺ specificity to the enzyme [23], due to the unfavorable charge–charge interactions with the 2'-phosphate of NADP⁺. This residue is topologically equivalent to residue 345 in mNAD-ME, which is conserved as aspartate in all the ME sequences irrespective of their cofactor specificity. In the mNAD-ME structure, the sidechain of Asp345 points away from the ribose ($\chi_1 = 56^\circ$ as compared to -157° in 1PSD). This conformation might explain the dual-specificity of mNAD-ME,

and the NADP⁺ dependence of other MEs with a conserved aspartate at this position.

The adenine ring of NAD⁺ is on the surface of the protein and positioned between the sidechain of the residue immediately following the conserved aspartate in the primary sequence (Lys346 in mNAD-ME) and that of the last residue in strand β 4 (Ala393 in mNAD-ME; Figure 2c). No specific recognition of the N1 and N6 atoms of adenine was observed. The nicotinamide ring is located deeper in the structure, at the interface between domains C, B and A. The amido nitrogen of the nicotinamide group is recognized by two hydrogen bonds with the protein, involving the mainchain carbonyl of residue 465 and the sidechain of Asn467 (from the linker between domains B and C). Gly446 is located close to this amide group and is strictly conserved among MEs. Mutation of the equivalent Gly444 residue of *Saccharomyces pombe* ME to an aspartate inactivated the enzyme [40].

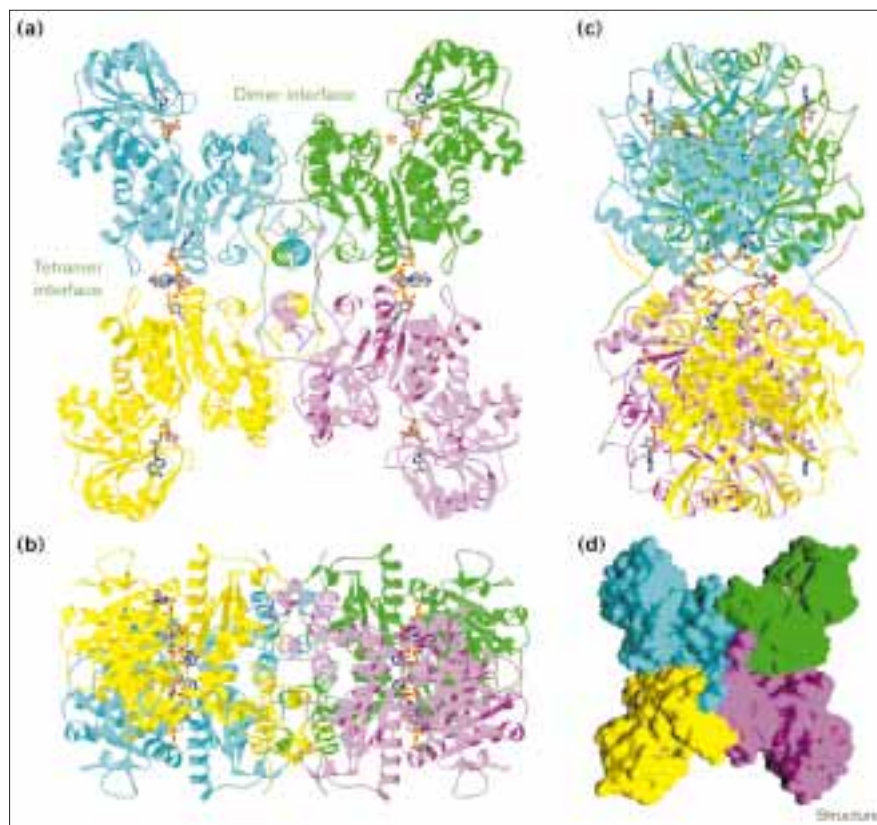
The tetramer

The tetramer of mNAD-ME obeys 222 point group symmetry (Figure 4) [41], and each monomer in the tetramer has essentially the same environment. The four monomers are arranged in the planar rather than tetrahedral fashion; this arrangement was also observed in electron microscopy

studies of pigeon liver ME [42]. The dimensions of the tetramer are $\sim 110 \text{ \AA} \times 110 \text{ \AA} \times 55 \text{ \AA}$, consistent with electron microscopy [42] and solution light-scattering studies [41].

The formation of the tetramer gives rise to the burial of $\sim 2900 \text{ \AA}^2$ surface area for each monomer. Of this, 1800 \AA^2 is rendered inaccessible to solvent upon the formation of the dimer and 1100 \AA^2 is buried at the tetramer interface. The dimer interface is contiguous, with intimate association of the two monomers (Figure 4). In comparison, the association between the two dimers appears to be rather loose, and there are solvent channels at the interface. The tetramer therefore appears to be a dimer of dimers. This is consistent with biochemical studies, which showed that ME exists in a monomer \leftrightarrow dimer \leftrightarrow tetramer equilibrium in solution [43]. Earlier kinetic and substrate-binding studies on the tetramer of pigeon liver ME showed that only two of the four active sites of the tetramer were catalytically competent [1]. An asymmetric model for the pigeon liver ME tetramer was proposed [44], requiring head-to-tail packing of the two dimers to cover up two of the active sites in the tetramer. A tetramer with such head-to-tail packing will not obey 222 point group symmetry, however, and is therefore inconsistent with the tetramer structure observed here for human mNAD-ME.

Figure 4



The tetramer of mNAD-ME. **(a)** Schematic drawing of the tetramer of human mNAD-ME, looking down the (crystallographic) twofold axis. The monomers are colored in green, cyan, yellow and purple. The bound NAD⁺ molecules are shown in stick representation. The active site of one monomer is indicated by a red star. The dimer and tetramer interfaces are labeled. **(b)** The structure of the tetramer, after 90° rotation around the horizontal axis, showing the intimate association at the dimer interface. **(c)** The tetramer after a 90° rotation around the vertical axis, looking down the tetramer interface. Ignoring the nicotinamide rings of the second NAD⁺ molecule, which are disordered in the structure, there are solvent channels between the two dimers. **(d)** Molecular surface representation of the tetramer [66], in the same view and color scheme as (a).

The dimer interface involves residues from domains A and B of the monomer (Figure 3). Helices $\alpha A3$ and $\alpha A4$ run parallel to the twofold axis of the dimer and are located at the dimer interface. There is a mainchain hydrogen bond from the carbonyl of residue 52 (in the loop between helices $\alpha A2$ and $\alpha A3$) to the amide of residue 134 (in strand $\beta B1$ of the other monomer). Four charged sidechains from one monomer (Glu90, Arg91, Arg128 and Arg129) are located close to their symmetry-mates in the other monomer, forming a highly polar interface at the dimer twofold axis.

Most of the 1100 Å² surface area of each monomer that becomes buried on tetramer formation is mediated by the long, extended segment at the C terminus of the protein (residues 566–573). This segment reaches into the other dimer of the tetramer and interacts with residues in both monomers of that dimer. This interface provides ~950 Å² of the buried surface area and therefore appears to be the driving force for tetramerization. The four C-terminal tails are arranged as two pairs, both of which are located near the (crystallographic) twofold axis of the tetramer (Figure 4). A hydrophobic core is formed by residues in each pair (Leu566, Pro567, Val569 and their symmetry mates), together with residues from helix $\alpha A2$ (Gln43, Met47 and Leu48). The sidechains of Tyr570 and Trp572 are each located in a hydrophobic pocket at the interface of the other dimer, involving residues from domain A ($\alpha A2$ and the $\alpha A2$ – $\alpha A3$ connection) of one monomer and residues from domain B (the $\beta B1$ – $\alpha B1$ loop and $\alpha B1$) of the other monomer. A second interface is located at the other (non-crystallographic) twofold axis of the tetramer, where residues 541–FRYP–544 are related to their symmetry mates. This interface contributes ~150 Å² to the total buried surface area. Finally, residues 23–24 are located near the (crystallographic) twofold axis of the tetramer. These residues have rather weak electron density, however, and their actual contribution to the tetramer interface is difficult to ascertain.

Residues that form the dimer interface of mNAD-ME show good conservation among the various MEs (Figure 3). The dimer interface observed here for mNAD-ME may be maintained in most MEs. The C-terminal segment, which appears to be the driving force for formation of the observed tetramer, is conserved among animal MEs, but shows significant variability in MEs from plants, yeast and bacteria. For example, the maize ME sequence stops at residue 566 [45], and the tetramerization of this protein may occur through a different structural mechanism. It might also be possible that the tetramer observed here is not the most stable form of this oligomer for mNAD-ME, owing to the binding of the second NAD⁺ molecule.

The sidechain of residue Phe40, which is strictly conserved among all the MEs, is located in the center of the hydrophobic core between helices $\alpha A1$ and $\alpha A2$. Substitution of its equivalent residue in pigeon liver ME with smaller residues

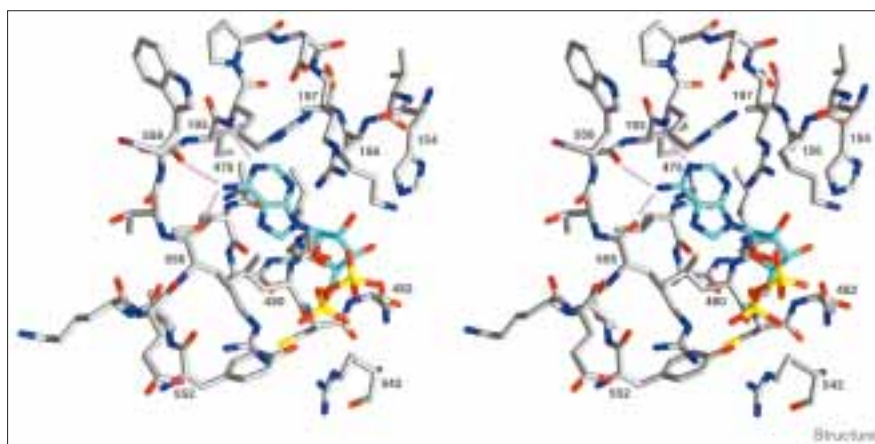
(alanine or glycine) resulted in mutants that are monomeric in solution, whereas substitution with tyrosine had little effect [46]. These experimental observations are in agreement with the current structure. Removal of the phenylalanine sidechain may destroy the hydrophobic core, thus destabilizing the conformations of the two helices and the loops connected to them. These residues are crucial for the formation of the dimer and tetramer interfaces, even though Phe40 itself is not at the interface (Figure 3).

A second NAD⁺-binding site

It was expected that there would be one NAD⁺-binding site in each monomer of the enzyme. However, the structure clearly shows the presence of a second NAD⁺ molecule in each monomer. This second molecule is located near the N-terminal end of the parallel β sheet in domain B, and residues from domain D are also involved in the binding (Figure 5). The binding of a nucleotide near the N-terminal end of a parallel β sheet is rather unusual and has been observed only rarely. This NAD⁺ molecule is separated from the one in the active site by a distance of ~35 Å. The nicotinamide ring and its ribose have very weak electron density, suggesting that they are mostly disordered in the structure. In the current model, they are located in a solvent channel between the two dimers of the tetramer (Figure 4). The binding of this NAD⁺ molecule is therefore mediated by the ADP portion of the molecule, with the adenine ring buried in the protein. It might also be possible that the bound molecule is actually ADP, a hydrolysis product of NAD⁺. The N6 amino group of the adenine base makes two hydrogen bonds with the main-chain carbonyls of residues 192 (with a hydrogen-bonding distance of 2.5 Å) and 556 (3.3 Å). The N1 ring nitrogen makes a hydrogen bond to the mainchain amide of residue 194 (2.8 Å). This pattern of interactions appears to provide a specific recognition for the adenine base, and binding of other bases at this position is likely to be less favorable. The first phosphate group (equivalent to the α -phosphate of ATP) forms electrostatic interactions with the sidechains of Arg542 and Arg556. The second phosphate group (the β -phosphate) interacts with the sidechains of His154 and Arg197. The Arg197 sidechain is also involved in an amino–aromatic interaction with the adenine base [47].

This second NAD⁺-binding site is unlikely to be catalytic. The biological function, if any, of NAD⁺ binding to this second site is currently unknown. The identity of the natural ligand(s) of this binding site is also unknown. However, the structure does suggest that this second site could be for binding ATP, which is an allosteric inhibitor of mNAD-ME. ATP does not have any effects on the catalytic activity of the other two human ME isoforms. In this regard, none of the three arginine residues (Arg197, Arg542, Arg556) that are important for this binding site are present in the other two isoforms, or the other MEs. This suggests that the second binding site may not exist in

Figure 5



Stereoview drawing showing the second NAD⁺-binding pocket. Only the ADP portion of the NAD⁺ molecule is shown, with carbon atoms in cyan. Residues from the protein are shown with carbon atoms in gray. The hydrogen bonds from the N1 and N6 atoms of the adenine base are shown as dotted purple lines.

cNADP-ME and mNADP-ME, giving additional support for this site being the allosteric inhibitor site. Further biochemical and biophysical studies are needed to fully characterize the biological relevance of this second site.

The active site

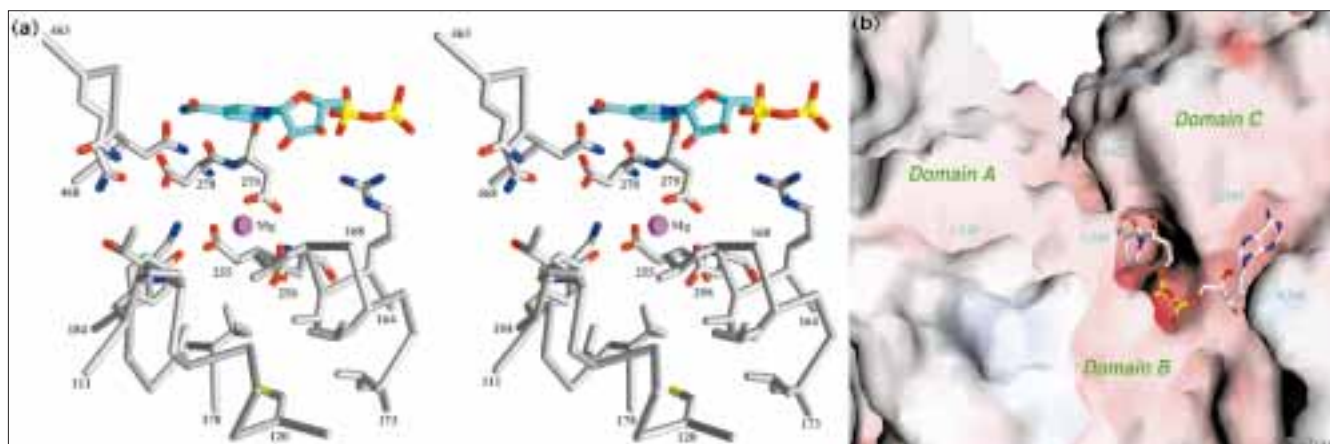
The nicotinamide ring of the first NAD⁺ molecule, associated with domain C, is located in a deep cleft in the structure at the interface between domains B and C in each monomer (Figures 1 and 6). This area is likely to be the active site of the enzyme. The two domains are positioned such that the C-terminal ends of their parallel β sheets point towards this active-site region. In addition, several residues from helix α A6 in domain A are also located close to the active site. The four active sites in the tetramer are separated from each other by a distance of ~ 60 Å, with the individual active sites located ~ 30 Å from the dimer or tetramer interface (Figure 4). Direct interactions between the active sites are therefore unlikely. Allosteric interactions among the active sites can give rise to cooperativity, as is the case with mNAD-ME, or possibly anticooperativity, which has been proposed for pigeon liver ME [48]. Such interactions may be mediated by helix α A6, which packs against helices α A3 and α A4 in the dimer interface. It should be noted, however, that many MEs, such as human cNADP-ME and mNADP-ME, do not display any cooperative behavior.

Despite the presence of Mg²⁺ and the substrate analog tartronate in the crystallization solution, neither are bound to the enzyme in the crystal. This suggests that the conformation of mNAD-ME may be an 'open' state. The presence of the second NAD⁺ molecule in the putative site for the allosteric inhibitor ATP is consistent with this interpretation. Further structural studies are needed to determine whether the binding of the cation and the substrate induces a 'closed' conformation of the enzyme.

There is a cluster of three strictly conserved acidic residues near the nicotinamide ring — Glu255, Asp256 and Asp279. Residues Glu255 and Asp256 are located near the C-terminal end of strand β B4 in domain B, and residue Asp279 is located near the beginning of helix α C0 in domain C. It is possible that these three residues are ligands for the divalent cation that is required for ME catalysis (Figure 6). The identification of Asp279 as a ligand for the cation is consistent with previous observations based on Fe-ascorbate affinity cleavage and site-specific mutagenesis studies on the pigeon liver cNADP-ME [49,50]. Affinity cleavage with the Cu-ascorbate system identified three additional residues as possible ligands for the cation [51], corresponding to Asp162, Asp215 and Asp488 in mNAD-ME. However, none of these three aspartate residues are located near the Asp279 residue in the structure.

Besides the acidic residues mentioned above, several segments of the protein structure participate in the formation of the active site. These segments correspond to highly conserved regions in the amino acid sequences of MEs (Figure 3), giving further support for their presence in the active site. From domain A, helix α A6 contributes residues 112-YTPXVGXXCS-121, where X represents an amino acid with its sidechain pointing away from the active site. The strictly conserved Tyr112 residue, is part of the bulge in this helix, and its sidechain hydroxyl group is located close to the cluster of the three acidic sidechains (Figure 6). Tyr112 may also be a ligand for the divalent cation, or it may have a different role in catalysis. The sidechain of Cys120 is ~ 17 Å away from the nicotinamide ring (Figure 6). Its equivalent in duck liver ME can be covalently modified by the substrate analog bromopyruvate, and the modification eliminated the binding of malate without affecting the binding of NADP⁺ cofactor [52]. The structure shows that the effect of Cys120 modification on malate binding is likely to be indirect. From domain B, residues 165-RILGL-169 (in the β B2'– β B3'

Figure 6



The active site of mNAD-ME. (a) Stereoview drawing showing the active-site region of mNAD-ME. Protein residues are shown with carbon atoms in gray. The nicotinamide ribose of the NAD⁺ molecule is shown with carbon atoms in cyan; phosphorus atoms are in yellow. To illustrate the location of the cation-binding site, a magnesium ion has been modeled into the structure (shown as a magenta sphere). The GLGDLG

motif corresponds to residues 168–173. (b) The molecular surface of human mNAD-ME near the active-site region [66]. The surface is colored on the basis of electrostatic potential: red, negative; blue, positive; white, neutral. The NAD⁺ molecule is shown as a stick model colored according to atom type. The three domains of the enzyme are labeled, as are the positions of several residues in this active-site region.

hairpin) and 176-GXXIPXXK-183 (helix α B2) are located near the active site. The Arg165 sidechain interacts with the diphosphate group of the NAD⁺ cofactor, although this residue shows nonconservative substitutions to glycine and serine in the yeast and *B. subtilis* MEs. Residues 161–173 correspond to one of the most conserved regions in MEs and include the GLGDLG motif. The strictly conserved Lys183 sidechain interacts with that of Asp278 (the first residue of α C0) and Glu255. Asp278 is conserved except for a plant ME, where it is a valine. From domain C, residues 421-NPT-423 (in the β C5– α C5 connection, with Pro422 in the *cis* conformation) and 446-GSP-448 (in the loop after β C6) may be involved in substrate binding. Finally, residues 464-QXNNVXXF-471, at the boundary between domains B and C, contribute three conserved sidechain amide groups to the active-site region. The sidechain of Asn467 is also involved in recognition of the nicotinamide group, as discussed earlier.

In addition to Cys120, chemical modification studies have indicated the presence of arginine and tyrosine residues in the active site of various MEs, although the identity of the residues were not determined from these studies. Modification of one tyrosine sidechain of pigeon liver ME resulted in loss of enzyme activity [53]. On the basis of the crystal structure, this might correspond to Tyr112 of mNAD-ME. Modification of one arginine residue in pigeon liver ME and maize ME eliminated the binding of malate without affecting the binding of the NADP⁺ cofactor [54,55]. This suggested that an arginine residue might be involved in malate binding. In the current structure, there is only one arginine residue (Arg165) near the active

site. Its sidechain is close to the phosphates of the cofactor and may be too far from the substrate. However, the conformation of this sidechain might be different in the 'closed' state of the enzyme, when the substrate is bound. Overall, the active-site region in mNAD-ME contains only two positively charged residues, Lys183 and Arg165, and the latter is not strictly conserved among MEs. This suggests that ionic interactions might not be a major component for the binding of the dicarboxylic malate substrate. This is in contrast to the binding of isocitrate to ICDH, where the C1 carboxylate group interacts with three arginine residues [56].

The nicotinamide ring is in the *anti* conformation, with the B face packed against residues in domain C (Figure 6). This conformation is stabilized by specific recognition of the amide group on the ring, notably by the conserved Asn467 sidechain. Therefore, MEs are expected to have A-type stereospecificity for hydride transfer to the dinucleotide cofactor.

Discussion

The allosteric control of human mNAD-ME is consistent with its role in the glutaminolysis pathway. Fumarate and succinate are products from the previous two steps in this pathway, and their activation of mNAD-ME can help ensure that there is sufficient ME activity when the pathway is on. On the other hand, ATP is a universal currency of free energy in biological systems [8]. Its inhibition of mNAD-ME may prevent the generation of excess energy molecules. A similar allosteric control mechanism has been observed for pyruvate kinase, which catalyzes

the last reaction in glycolysis. The L isoform of this enzyme is allosterically activated by fructose 1,6-bisphosphate, the product from the preceding irreversible step in the pathway, and is allosterically inhibited by ATP [8]. Such a comparison offers additional support for the glutaminolysis pathway, and for the importance of mNAD-ME in energy metabolism. The activity level of this enzyme in the Morris hepatoma is correlated with the progression of the malignancy, indicating that energy production in these tumor cells may be dependent on mNAD-ME [13,14,57].

Human mNAD-ME displays cooperativity with respect to the substrate malate. On the basis of the concerted model for allosteric interactions, the enzyme tetramer may exist in a catalytically competent R state and a T state, which has significantly lower affinity for the substrate. The binding of the allosteric inhibitor (ATP) stabilizes the T state and reduces the enzyme activity. The presence of a second NAD⁺ molecule in the structure, which possibly mimics the binding of ATP, suggests that the current structure may represent the T state of the enzyme. However, an anticooperativity has been proposed for the pigeon liver ME [48], which cannot be explained by the concerted model. The current structure shows that the tetramer of mNAD-ME may be a dimer of dimers, and it would be interesting to establish whether the allosteric interactions occur only within the dimers. In this regard, preliminary kinetic experiments showed that the Hill coefficient of the enzyme with respect to malate, in the absence of fumarate, is ~1.5 (GB and LT, unpublished data). An understanding of the structural basis of the cooperative behavior will have to await further studies.

Catalysis by MEs generally proceeds in two steps — the dehydrogenation of malate to produce oxaloacetate (the same reaction as that catalyzed by MDH), and decarboxylation to produce pyruvate [5]. A general base is needed for the first step to extract the proton for dehydrogenation, and a general acid is needed for the second step to protonate the product of decarboxylation. In the functionally related enzyme ICDH, which also has a two step catalytic mechanism, one of the aspartate ligands of the cation was proposed as the general base and a tyrosine or lysine residue was proposed as the general acid [56]. The situation with ME is more complicated, as a water-mediated interaction between the cation and the substrate is expected [4,58]. This might increase the distance between the aspartate/glutamate ligands of the cation and malate, making them less likely to function as the general base. At the same time, the bridging water molecule could be a good candidate for the general base. For the general acid, the structure of mNAD-ME also contains a tyrosine and a lysine residue in close proximity in the active site (Figure 6). Further studies, especially the determination of a structure of the holoenzyme, are needed to fully characterize the functions of these and other residues in catalysis.

NAD⁺-dependent enzymes are generally associated with oxidative metabolic processes, and NADP⁺-dependent enzymes are generally associated with reductive biosynthesis. The structural basis for this selectivity/specificity towards the cofactor by the various enzymes is still not well understood. Earlier studies suggested two specificity determinants for enzymes that contain Rossmann folds [19,23]. The presence of a GXGXXG signature motif indicates NAD⁺ specificity, whereas a GXGXXA motif indicates NADP⁺ specificity. Secondly, the presence of an acidic residue near the end of strand β 2 of the Rossmann fold indicates NAD⁺ specificity, as this residue recognizes the hydroxyl groups on the ribose. ME appears to violate both of these 'rules'. A GXGXXA motif is present in all animal MEs, whereas a GXGXXG motif is present in all plant, yeast and bacterial MEs, irrespective of their cofactor specificity. In addition, an aspartate residue is conserved in all MEs at the end of β 2, corresponding to Asp345 of human mNAD-ME. The current structure shows that this sidechain points away from the ribose, providing a possible mechanism for NADP⁺ binding even in the presence of this acidic residue. It is not known why the Asp345 sidechain points away in this NAD⁺ complex. mNAD-ME has comparable affinity for NAD⁺ and NADP⁺, with that for NADP⁺ being about two to fivefold weaker than for NAD⁺ [2]. mNAD-ME is a dual-specificity enzyme, and our experiments with NADP⁺ binding to this enzyme suggest that there may be little conformational differences between the NAD⁺ and NADP⁺ complexes of this enzyme. Comparative studies between this dual-specificity isoform and the NADP⁺-specific isoforms of human ME may lead to a greater understanding of the structural basis of cofactor specificity.

Biological implications

Malic enzymes are widely distributed in nature and have important biological functions. Their amino acid sequences show no recognizable homology to those of other oxidative decarboxylases or to other proteins in general. This first structure of a malic enzyme confirms that it belongs to a new class of oxidative decarboxylases, with a distinct backbone structure. Malic enzymes have been studied extensively by biochemical, kinetic and mutagenesis experiments. The crystal structure of human mitochondrial NAD(P)⁺-dependent malic enzyme reported here provides an explanation, at the molecular level, to many of these prior observations.

The active site of the enzyme is located in a deep cleft at the interface of three domains of the enzyme monomer; residues forming this active site are highly conserved. The nicotinamide ring of an NAD⁺ molecule, associated with a Rossmann fold domain, is located in this active-site region. The amino acid sequences of malic enzymes contain two dinucleotide-binding signature motifs (GXGXXG/A). The structure shows that only one of

these is involved in binding an NAD⁺ molecule. The other motif is located in the active site and may be involved in substrate binding. Catalysis by malic enzymes requires the presence of divalent cations (Mg²⁺ or Mn²⁺). On the basis of the crystal structure, three acidic residues (Glu255, Asp256 and Asp279) were identified as ligands for the cation. The identification of Asp279 as a ligand is consistent with earlier biochemical and mutagenesis studies.

The structure shows that the tetramer of the enzyme appears to be a dimer of dimers. This observation has potential implications for the allosteric control of the enzyme. It might be possible that dimers, rather than tetramers, are the units that display cooperative behavior. A glimpse into the possible mechanism of allosteric control of this enzyme is provided by the observation of NAD⁺ binding to a second site, the natural ligand of which may be the allosteric inhibitor ATP.

Materials and methods

Protein expression, purification and crystallization

Details of the expression, purification and crystallization of human mNAD-ME will be presented elsewhere [41]. Briefly, mNAD-ME was over-expressed in *E. coli* and purified by anion exchange, ATP affinity and gel-filtration chromatography [3]. Crystals of mNAD-ME were obtained at 4°C by the hanging-drop vapor diffusion method. Many different crystal forms were observed [41]. Crystals used for the current structure analysis belong to space group B2, with cell parameters of $a = 204.4 \text{ \AA}$, $b = 107.0 \text{ \AA}$, $c = 59.2 \text{ \AA}$ and $\gamma = 101.9^\circ$. There is a dimer of mNAD-ME in the asymmetric unit, giving a V_m of $\sim 2.5 \text{ \AA}^3/\text{Da}$. For crystallization, the protein concentration was 8 mg/ml, in a buffer containing 30 mM Tris (pH 7.4), 125 mM KCl, 3 mM NAD⁺ and 10 mM DTT. The reservoir solution contained 100 mM Hepes (pH 7.0), 8% PEG 8000, 5% MPD, 6 mM MgSO₄ and 10 mM tartrate.

Structure determination

The structure was determined by the selenomethionyl MAD method [29]. The selenomethionyl protein was expressed in *E. coli* in a defined media, purified and crystallized using protocols that are essentially the same as for the wild-type protein. The catalytic activity of the selenomethionyl protein was comparable to that of the wild-type enzyme, suggesting that the selenomethionyl residues did not have any major impact on the structure of the enzyme. The MAD data set, to 2.5 Å resolution, was collected at beamline X4A of the National Synchrotron Light Source (NSLS) at Brookhaven National Laboratory. The crystal was maintained at cryotemperature and the entire data set was collected with one crystal, measuring $0.5 \times 0.2 \times 0.08 \text{ mm}^3$. Four wavelengths were used for the MAD data collection: λ_1 (12550 eV, 0.9879 Å wavelength, remote), λ_2 (12660 eV, 0.9793 Å, edge), λ_3 (12663 eV, 0.9791 Å, peak) and λ_4 (12800 eV, 0.9686 Å, remote). Inverse beam geometry was used to collect the Friedel pairs. The diffraction images were recorded on an R-Axis IV imaging plate detector, and processed with DENZO and SCALEPACK [59]. The oscillation range per frame was 2°, and the exposure time per frame was ~4 min. The crystal was aligned with the twofold c axis along the X-ray beam and the long a axis along the spindle before the start of data collection. A total of 90° oscillation (together with 90° for the inverse beam portion) was collected for each wavelength.

The reflection data sets from the four wavelengths were loaded into the MADSYS program package [29]. The statistics from the MAD analysis were excellent (Tables 1 and 2), confirming the quality of the

Table 1

Data processing statistics for MAD data set at λ_4 .

Resolution (Å)	R _{merge} (%)	Completeness (%)
4.0	3.2	95
3.5	4.3	94
3.0	6.7	94
2.5	11.5	72

MAD data set and suggesting that the F_A values were likely to be good estimates for the scattering of the Se atoms. There are 14 methionine residues in each monomer (excluding the initiator methionine residue), therefore a total of 28 Se sites are expected in the asymmetric unit. Earlier experience with the structure determination of other proteins have raised some doubts as to the likelihood of success with the F_A approach with these many Se sites [60]. However, by careful selections of input parameters to the program SHELXS-86 (G Sheldrick) and examinations of its outputs, we were able to solve the positions of the Se sites with direct methods. The F_A values in the resolution range of 30–3.5 Å were used in the calculation, which revealed the positions of all 28 Se sites.

The phase information to 2.5 Å resolution from the MAD analysis was improved by solvent flattening and twofold noncrystallographic symmetry (NCS) averaging with a local program (LT, unpublished). The electron-density map was of sufficient quality, allowing many residues of the protein to be located (Figure 7). The knowledge of the 14 Se sites, and therefore the 14 methionine positions in the molecule, provided independent confirmation for the trace. Residues 346–465 had weaker and less resolved electron density, suggesting flexibility for these residues. It was recognized that these residues may have a Rossmann fold, and the β strands in the Rossmann fold of lactate dehydrogenase (PDB entry 1LDM) [39] were manually overlaid into the electron density. This helped the tracing for this domain of the structure. The model of the protein was built into the electron density with the program O [61].

Locating NAD⁺-binding sites

In order to provide an independent observation for the position of the NAD⁺ molecule in the protein, we took advantage of the 'dual-specificity' of mNAD-ME. Crystals of the enzyme were grown in the presence of NADP⁺ instead of NAD⁺. An X-ray diffraction data set to 2.4 Å resolution was collected on such a crystal at the F2 beamline at Cornell High Energy Synchrotron Source (CHESS). These crystals are isomorphous to those of the NAD⁺ crystals, allowing a difference

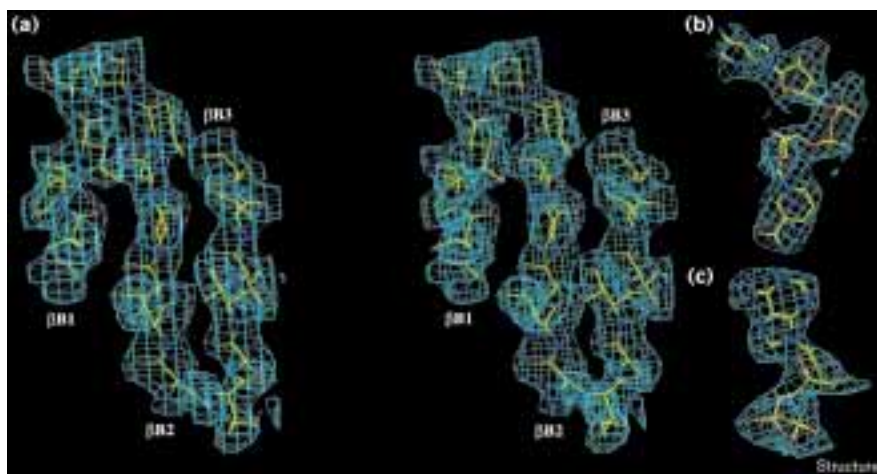
Table 2

Anomalous diffraction ratios* from the MAD analysis.

Wavelength	λ_1	λ_2	λ_3	λ_4
λ_1	4.9 (2.8)	4.2	3.6	4.1
λ_2	–	5.5 (2.9)	3.0	5.8
λ_3	–	–	7.8 (2.8)	4.3
λ_4	–	–	–	6.0 (2.7)

*Anomalous diffraction ratios (for 30–4 Å reflection data) are Bijvoet difference ratios along the diagonal (with those for centric reflections shown in parentheses); dispersive difference ratios off-diagonal. The ratios are given as percentages. For phasing, $\Delta(\Delta\phi) = 30^\circ$ and $R(F_A) = 32\%$, where $\Delta(\Delta\phi)$ is the average difference between independent determinations of $\Delta\phi$ from the MAD analysis [29].

Figure 7



Electron density for the mNAD-ME structure after MAD phasing and twofold noncrystallographic averaging at 2.5 Å resolution. The contour level is at 0.75σ. (a) Stereoview electron-density map for some of the β sheet residues in domain B. The electron density for (b) the NAD⁺ molecule in the active site of the enzyme and (c) the second NAD⁺ molecule, with only the ADP portion shown.

electron-density map to be calculated. The map is expected to contain peaks corresponding to the phosphate groups of the NADP⁺ molecules. Surprisingly, two peaks were identified in each monomer of mNAD-ME in the difference map. One of them is associated with the Rossmann fold and belongs to the NADP⁺ molecule bound to it. The other peak is associated with an unexpected second binding site for NAD(P)⁺ in mNAD-ME.

Structure refinement

The structure refinement was carried out with the program X-PLOR [62], using a native data set to 2.1 Å resolution that was collected on a CCD detector at the F2 beamline of CHESS. NCS restraints were used throughout the structure refinement, initially on all the atoms and finally on only the Cα atoms. Residues Gln335 and Lys339 in both monomers, and residues Lys352 and Arg354 in the first monomer, are modeled as alanines due to lack of sidechain electron density. The statistics on the quality of the native reflection data set and the structure refinement are summarized in Table 3.

Accession numbers

The atomic coordinates for mNAD-ME have been deposited in the Protein Data Bank with accession code 1QR6.

Table 3

Summary of refinement statistics.

Maximum resolution (Å)	2.1
No. of observations	343,811
No. of unique reflections	70,337
R _{merge} (%)	4.3
Resolution range for refinement (Å)	20–2.1
No. of reflections in refinement (F > 2σ)	64,039
Reflection data completeness (%)	87
R factor (%) [*]	22.8
R _{free} (%) [†]	28.7
Rms deviation in bond lengths (Å)	0.008
Rms deviation in bond angles (°)	1.4
No. of protein residues	1102
No. of protein atoms	8676
No. of NAD ⁺ residues	4
No. of NAD ⁺ atoms	176
No. of solvent atoms	760

^{*}R = $\sum_h |F_h^o - F_h^c| / \sum_h F_h^o$. [†]R_{free} was calculated for 7.5% of the reflection data.

Acknowledgements

We thank Craig Ogata for setting up the beamline at NSLS, Young Chul Park for help with data collection at CHESS, Wayne Hendrickson for many helpful discussions, Suet Mui and Susan Pav for contributions in the earlier stages of this project and Mary Ann Gawinowicz for the MALDI-TOF analysis on the protein samples.

References

- Hsu, R.Y. (1982). Pigeon liver malic enzyme. *Mol. Cell. Biochem.* **43**, 3-26.
- Moreadith, R.W. & Lehninger, A.L. (1984). Purification, kinetic behavior, and regulation of NAD(P)⁺ malic enzyme of tumor mitochondria. *J. Biol. Chem.* **259**, 6222-6227.
- Loeber, G., Infante, A.A., Maurer-Fogy, I., Krystek, E. & Dworkin, M.B. (1991). Human NAD⁺-dependent mitochondrial malic enzyme. *J. Biol. Chem.* **266**, 3016-3021.
- Tipton, P.A., Quinn, T.P., Peisach, J. & Cook, P.F. (1996). Role of the divalent metal ion in the NAD:malic enzyme reaction: an ESEEM determination of the ground state conformation of malate in the E:Mn:malate complex. *Protein Sci.* **5**, 1648-1654.
- Urbauer, J.L., Bradshaw, D.E. & Cleland, W.W. (1998). Determination of the kinetic and chemical mechanism of malic enzyme using (2R,3R)-erythro-fluoromalate as a slow alternative substrate. *Biochemistry* **37**, 18026-18031.
- Ochoa, S., Mehler, A. & Kornberg, A. (1947). Reversible oxidative decarboxylation of malic acid. *J. Biol. Chem.* **167**, 871-872.
- Loeber, G., Maurer-Fogy, I. & Schwendenwein, R. (1994). Purification, cDNA cloning and heterologous expression of the human mitochondrial NAD⁺-dependent malic enzyme. *Biochem. J.* **304**, 687-692.
- Stryer, L. *Biochemistry*. (1995). WH Freeman & Company, New York, NY.
- Moore, P.D. (1982). Evolution of photosynthetic pathways in flowering plants. *Nature* **295**, 647-648.
- Borsch, D. & Westhoff, P. (1990). Primary structure of NADP-dependent malic enzyme in the dicotyledonous C4 plant *Flaveria trinervia*. *FEBS Lett.* **273**, 111-115.
- Wynn, J.P., Kendrick, A., Hamid, A.A. & Ratledge, C. (1997). Malic enzyme: a lipogenic enzyme in fungi. *Biochem. Soc. Trans.* **25**, S669.
- Goodridge, A.G., et al., & Roncero, C. (1996). Nutritional and hormonal regulation of expression of the gene for malic enzyme. *Prog. Nucl. Acid Res. Mol. Biol.* **52**, 89-122.
- Sanz, N., Diez-Fernandez, C., Valverde, A.M., Lorenzo, M., Benito, M. & Cascales, M. (1997). Malic enzyme and glucose 6-phosphate dehydrogenase gene expression increases in rat liver cirrhogenesis. *Br. J. Cancer* **75**, 487-492.
- Baggetto, L.G. (1992). Deviant energetic metabolism of glycolytic cancer cells. *Biochimie* **74**, 959-974.
- McKeehan, W.L. (1982). Glycolysis, glutaminolysis and cell proliferation. *Cell Biol. Int. Rep.* **6**, 635-650.
- Reitzer, L.J., Wice, B.M. & Kennell, D. (1979). Evidence that glutamine, not sugar, is the major energy source for cultured HeLa cells. *J. Biol. Chem.* **254**, 2669-2676.

17. Winning, B.M., Bourguignon, J. & Leaver, C.J. (1994). Plant mitochondrial NAD⁺-dependent malic enzyme. *J. Biol. Chem.* **269**, 4780-4786.
18. Kobayashi, K., Doi, S., Negoro, S., Urabe, I. & Okada, H. (1989). Structure and properties of malic enzyme from *Bacillus stearothermophilus*. *J. Biol. Chem.* **264**, 3200-3205.
19. Wierenga, R.K., Terpstra, P. & Hol, W.G.J. (1986). Prediction of the occurrence of the ADP-binding $\beta\alpha\beta$ -fold in proteins, using an amino acid sequence fingerprint. *J. Mol. Biol.* **187**, 101-107.
20. Adams, M.J., Ellis, G.H., Gover, S., Naylor, C.E. & Phillips, C. (1994). Crystallographic study of coenzyme, coenzyme analogue and substrate binding in 6-phosphogluconate dehydrogenase: implications for NADP specificity and the enzyme mechanism. *Structure* **2**, 651-668.
21. Hurley, J.H., Dean, A.M., Sohl, J.L., Koshland, D.E., Jr. & Stroud, R.M. (1990). Regulation of an enzyme by phosphorylation at the active site. *Science* **249**, 1012-1016.
22. Imada, K., Sato, M., Tanaka, N., Katsube, Y., Matsuura, Y. & Oshima, T. (1991). Three-dimensional structure of a highly thermostable enzyme, 3-isopropylmalate dehydrogenase of *Thermus thermophilus* at 2.2 Å resolution. *J. Mol. Biol.* **222**, 725-738.
23. Scrutton, N.S., Berry, A. & Perham, R.N. (1990). Redesign of the coenzyme specificity of a dehydrogenase by protein engineering. *Nature* **343**, 38-43.
24. Baker, P.J., Britton, K.L., Rice, D.W., Rob, A. & Stillman, T.J. (1992). Structural consequences of sequence patterns in the fingerprint region of the nucleotide binding fold. *J. Mol. Biol.* **228**, 662-671.
25. Hurley, J.H., Chen, R. & Dean, A.M. (1996). Determinants of cofactor specificity in isocitrate dehydrogenase: Structure of an engineered NADP⁺→NAD⁺ specificity-reversal mutant. *Biochemistry* **35**, 5670-5678.
26. Sauer, L.A. (1973). An NAD- and NADP-dependent malic enzyme with regulatory properties. *Biochem. Biophys. Res. Commun.* **50**, 524-531.
27. Baker, P.J., Thomas, D.H., Barton, C.H., Rice, D.W. & Bailey, E. (1987). Crystallization of an NADP⁺-dependent malic enzyme from rat liver. *J. Mol. Biol.* **193**, 233-235.
28. Clancy, L.L., et al., & Einspahr, H.M. (1992). Crystallization of the NAD-dependent malic enzyme from the parasitic nematode *Ascaris suum*. *J. Mol. Biol.* **226**, 565-569.
29. Hendrickson, W.A. (1991). Determination of macromolecular structures from anomalous diffraction of synchrotron radiation. *Science* **254**, 51-58.
30. Rossmann, M.G., Moras, D. & Olsen, K.W. (1974). Chemical and biological evolution of a nucleotide binding protein. *Nature* **250**, 194-199.
31. Holm, L. & Sander, C. (1993). Protein structure comparison by alignment of distance matrices. *J. Mol. Biol.* **233**, 123-138.
32. Murzin, A.G., Brenner, S.E., Hubbard, T. & Chothia, C. (1995). SCOP: a structural classification of proteins database for the investigation of sequences and structures. *J. Mol. Biol.* **247**, 536-540.
33. Schuller, D.J., Grant, G.A. & Banaszak, L.J. (1995). The allosteric ligand site in the V_{max}-type cooperative enzyme phosphoglycerate dehydrogenase. *Nature Struct. Biol.* **2**, 69-76.
34. Lamzin, V.S. et al. & Wilson, K.S. (1992). Crystal structure of NAD-dependent formate dehydrogenase. *Eur. J. Biochem.* **206**, 441-452.
35. Goldberg, J.D., Yoshida, T. & Brick, P. (1994). Crystal structure of a NAD-dependent D-glycerate dehydrogenase at 2.4 Å resolution. *J. Mol. Biol.* **236**, 1123-1140.
36. Dengler, U., Niefind, K., Kiess, M. & Schomburg, D. (1997). Crystal structure of a ternary complex of D-2-hydroxyisocaproate dehydrogenase from *Lactobacillus casei*, NAD⁺ and 2-oxoisocaproate at 1.9 Å resolution. *J. Mol. Biol.* **267**, 640-660.
37. Stillman, T.J., et al., & Rice, D.W. (1999). Insights into the mechanism of domain closure and substrate specificity of glutamate dehydrogenase from *Clostridium symbiosum*. *J. Mol. Biol.* **285**, 875-885.
38. Baker, P.J., Turnbull, A.P., Sedelnikova, S.E., Stillman, T.J. & Rice, D.W. (1995). A role for quaternary structure in the substrate specificity of leucine dehydrogenase. *Structure* **3**, 693-705.
39. Abad-Zapatero, C., Griffith, J.P., Sussman, J.L. & Rossmann, M.G. (1987). Refined crystal structure of dogfish M4 apo-lactate dehydrogenase. *J. Mol. Biol.* **198**, 445-467.
40. Viljoen, M., van der Merwe, M., Subden, R.E. & van Vuuren, H.J. (1998). Mutation of Gly-444 inactivates the *S. pombe* malic enzyme. *FEMS Microbiol. Lett.* **167**, 157-162.
41. Bhargava, G., et al., & Tong, L. (1999). Preliminary crystallographic studies of human mitochondrial NAD(P)⁺-dependent malic enzyme. *J. Struct. Biol.*, in press.
42. Nevaldine, B.H., Bassel, A.R. & Hsu, R.Y. (1974). Mechanism of pigeon liver malic enzyme subunit structure. *Biochim. Biophys. Acta* **336**, 283-293.
43. Chang, G.-G., Huang, T.-M. & Chang, T.-C. (1988). Reversible dissociation of the catalytically active subunits of pigeon liver malic enzyme. *Biochem. J.* **254**, 123-130.
44. Lee, H.-J. & Chang, G.-G. (1990). Quarternary structure of pigeon liver malic enzyme. *FEBS Lett.* **277**, 175-179.
45. Rothermel, B.A. & Nelson, T. (1989). Primary structure of the maize NADP-dependent malic enzyme. *J. Biol. Chem.* **264**, 19587-19592.
46. Chou, W.-Y., Liu, M.-Y., Huang, S.-M. & Chang, G.-G. (1996). Involvement of Phe¹⁹ in the Mn²⁺-malate binding and the subunit interactions of pigeon liver malic enzyme. *Biochemistry* **35**, 9873-9879.
47. Burley, S.K. & Petsko, G.A. (1986). Amino-aromatic interactions in proteins. *FEBS Lett.* **203**, 139-143.
48. Pry, T.A. & Hsu, R.Y. (1980). Equilibrium substrate binding studies of the malic enzyme of pigeon liver. Equivalence of nucleotide sites and anticooperativity associated with the binding of L-malate to the enzyme-manganese(II)-reduced nicotinamide adenine dinucleotide phosphate ternary complex. *Biochemistry* **19**, 951-962.
49. Wei, C.-H., Chou, W.-Y., Huang, S.-M., Lin, C.-C. & Chang, G.-G. (1994). Affinity cleavage at the putative metal-binding site of pigeon liver malic enzyme by the Fe²⁺-ascorbate system. *Biochemistry* **33**, 7931-7936.
50. Wei, C.-H., Chou, W.-Y. & Chang, G.-G. (1995). Identification of Asp²⁵⁸ as the metal coordinate of pigeon liver malic enzyme by site-specific mutagenesis. *Biochemistry* **34**, 7949-7954.
51. Chou, W.-Y., Tsai, W.-P., Lin, C.-C. & Chang, G.-G. (1995). Selective oxidative modification and affinity cleavage of pigeon liver malic enzyme by the Cu²⁺-ascorbate system. *J. Biol. Chem.* **270**, 25935-25941.
52. Satterlee, J. & Hsu, R.Y. (1991). Duck liver malic enzyme: sequence of a tryptic peptide containing the cysteine residue labeled by the substrate analog bromopyruvate. *Biochim. Biophys. Acta* **1079**, 247-252.
53. Chang, G.-G. & Huang, T.-M. (1980). Involvement of tyrosyl residues in the substrate binding of pigeon liver malic enzyme. *Biochim. Biophys. Acta* **611**, 217-226.
54. Vernon, C.M. & Hsu, R.Y. (1983). Pigeon liver malic enzyme: involvement of an arginyl residue at the binding site for malate and its analogs. *Arch. Biochem. Biophys.* **225**, 296-305.
55. Rao, S.R., Kamath, B.G. & Bhagwat, A.S. (1991). Chemical modification of the functional arginine residue(s) of malic enzyme from *Zea mays*. *Phytochem.* **30**, 431-435.
56. Hurley, J.H., Dean, A.M., Koshland, D.E., Jr. & Stroud, R.M. (1991). Catalytic mechanism of NADP⁺-dependent isocitrate dehydrogenase: implications from the structures of Magnesium-isocitrate and NADP⁺ complexes. *Biochemistry* **30**, 8671-8678.
57. Sauer, L.A., Dauchy, R.T., Nagel, W.O. & Morris, H.P. (1980). Mitochondrial malic enzymes. *J. Biol. Chem.* **255**, 3844-3848.
58. Hsu, R.Y., Mildvan, A.S., Chang, G.-G. & Fung, C.-H. (1976). Mechanism of malic enzyme from pigeon liver. Magnetic resonance and kinetic studies of the role of Mn²⁺. *J. Biol. Chem.* **251**, 6574-6583.
59. Otwinowski, Z. (1993) Oscillation data reduction program. In *CCP4 Study Weekend: Data Collection and Processing*. (Sawyer, L., Isaacs, N. & Bailey, S., eds), pp56-62, SERC Daresbury Laboratory, Warrington, UK.
60. Turner, M.A., Yuan, C.-S., Borchardt, R.T., Hershfield, M.S., Smith, G.D. & Howell, P.L. (1998). Structure determination of selenomethionyl S-adenosylhomocysteine hydrolase using data at a single wavelength. *Nat. Struct. Biol.* **5**, 369-376.
61. Jones, T.A., Zou, J.Y., Cowan, S.W. & Kjeldgaard, M. (1991). Improved methods for building protein models in electron density maps and the location of errors in these models. *Acta Crystallogr. A* **47**, 110-119.
62. Brünger, A.T. (1992) *The X-PLOR manual*. Yale University Press, Yale, New Haven, CT.
63. Carson, M. (1987). Ribbon models of macromolecules. *J. Mol. Graph.* **5**, 103-106.
64. Birktoft, J.J. & Banaszak, L.J. (1983). The presence of a histidine-aspartic acid pair in the active site of 2-hydroxyacid dehydrogenase. *J. Biol. Chem.* **258**, 472-482.
65. Morioka, H., Magnuson, M.A., Mitsuhashi, T., Song, M.-K.H., Rall, J.E. & Nikodem, V.M. (1989). Structural characterization of the rat malic enzyme gene. *Proc. Natl Acad. Sci. USA* **86**, 4912-4916.
66. Nicholls, A., Sharp, K.A. & Honig, B. (1991). Protein folding and association: insights from the interfacial and thermodynamic properties of hydrocarbons. *Proteins* **11**, 281-296.